Fractional Brownian motion and anomalous diffusion in vibrated granular materials

J. Stat. Mech. (2012) P01002

(http://iopscience.iop.org/1742-5468/2012/01/P01002)

Journal of Statistical Mechanics: Theory and Experiment
An IOP and SISSA journal

Fractional Brownian motion and anomalous diffusion in vibrated granular materials

Alessandro L Sellerio, Daniele Mari and Gérard Gremaud

Groupe de Spectroscopie Mécanique, EPFL, CH-1015 Lausanne, Switzerland
E-mail: alessandro.sellerio@epfl.ch, daniele.mari@epfl.ch and gerard.gremaud@epfl.ch

Received 6 October 2011
Accepted 2 December 2011
Published 10 January 2012

Online at stacks.iop.org/JSTAT/2012/P01002
doi:10.1088/1742-5468/2012/01/P01002

Abstract. We propose a new approach to the study of diffusion dynamics in vibrated granular systems. The dynamic of a granular material is mainly defined by dry friction interactions. This type of interaction is difficult to model for a large quantity of particles. In this work, we study a granular system by analyzing the angular position time series of an immersed torsion oscillator and of an identical, torsionally unconstrained probe. In order to interpret the behavior of our mechanical system, the experiments are compared to simulations. We generate simulated time series using a simple model of a confined random walk. The global properties of the recorded signals, both experimental and simulated, are extracted by applying fractal signal processing analysis. We show that the Hurst exponent of the time series can be employed to discriminate the dynamics of the system. We conclude that the immersed probe behaves as a Brownian particle that can switch between three distinct dynamical regimes, depending on the strength of the torsional constraint applied to it. If the probe is strongly constrained, its trail can be described with a fractal Brownian motion showing anomalous diffusion (subdiffusive behavior). As the strength of the constraint is reduced, the system 'unjams' in a ordinary Brownian motion (normal diffusion). Finally, as the constraints are further reduced, we observe the onset of convection phenomena, which in turn induce a superdiffusive behavior.

Keywords: Brownian motion, granular matter, slow relaxation and glassy dynamics, jamming and packing

1742-5468/12/P01002+18$33.00

Contents

1. Introduction

Vibrated granular materials show a rich and complex phenomenology [1]. The relevant physical phenomena responsible for this complexity remain, however, largely unexplained [2]. In particular, it has been shown that the behavior of vibrated granular systems has strong similarities with the dynamics of glass-forming liquids [3]–[6].

Granular systems have been studied with a Langevin approach [7]. In the case of relatively strong vibrations, the material behaves like a fluid. The mechanical response function of the system was measured with the help of an externally driven torsion oscillator [8]. A relevant control parameter, acting as an effective temperature, is found to be the square of the relative vibration intensity Γ: $T_{\text{eff}} \propto \Gamma^2$. In this context, Γ is defined as the ratio between the average granular acceleration and gravity: $\Gamma = \langle a \rangle / g$.

As the vibration intensity decreases, the characteristic relaxation time diverge. In these conditions, the Langevin approach is not valid any more and other mechanisms dominate. The granular material starts to approach jamming as the subcooled liquid evolves into a glass [9]. These low energy conditions could also be studied with a torsion oscillator as in the case of the fluidized granular system. In this case, no external torque was applied to the probe: it was left free to move, while its angular position was recorded. The configurational noise spectrum was then studied [10, 9]. It shows a $1/f$ behavior, suggesting that, even when approaching jamming, we can expect a Brownian-like behavior.

These two approaches, however, do not yet suggest any interpretation on what happens in the system as we switch from the high vibration, fluid, regime, to the low vibration, jamming, regime. It is often supposed that vibrated granular materials show

J. Stat. Mech. (2012) P01002

Brownian-like behaviors, and sometimes this was used as a starting point for modeling [11]. On the other hand, little direct evidence of Brownian motion has been found in the case of large, three-dimensional granular media.

In this paper, we propose an analytical approach which demonstrates that macroscopic objects immersed in vibrated granular matter can indeed act as probes that behave as Brownian particles. The presence of constraints acting on the probe, both due to granular interactions or to external forces is observed. The applied technique is also experimentally significant since it allows an uninterrupted observation of the system as the jamming transition is crossed. The information that can be extracted in this case is potentially very interesting, as we still lack a way to define observables that are both physically relevant and easy to measure as we cross the jamming transition.

2. Methods

2.1. Simulation

As we will discuss briefly here and in section 2.2 that follows, our observations suggest a complex behavior where fractional Brownian motion and anomalous diffusion play a significant role. We performed simulations on a very simple model representing a constrained random walk. The purpose of the simulations is not to add anything new to this well-studied problem; instead they allow us to address two specific subject-matters. First, it is known that the fractal analysis of time series presents numerical difficulties. In this work, we use simulated data to assess the solidity of our data analysis techniques, when they are applied to sets of data over which we have full control. Second, part of our experimental results take place in a dynamic region where Brownian objects are submitted to an external, localizing, constraint. With the aid of simulations, we study, in controlled conditions, the behavior of such a system, so that we can relate the findings in experimental data.

We will now consider in more detail the key properties of our experimental configuration, that will need to be modeled and simulate. In our installation, a cylindrical probe is suspended in the granular system by the means of a relatively weak torsion spring. In this context, 'weak' means that the stiffness of the torsion spring is lower than the average stiffness of the non-vibrated granular. The assembly is sketched in figure 1 and discussed in details in section 2.2.

When the granular is vibrated, the probe behaves in a way similar to a (rotational) Brownian particle. This is due to the large number of interactions between the probe and the smaller grains. However, it is clear that the probe cannot move in a completely Brownian-like way. In fact, the torque that is transmitted to the probe at each collision (in the high vibration regime) or which can be transmitted by a local rearrangement of the chains of forces in the granular medium (in the low vibration regime) is finite. Therefore, there will be a limit angle (from the origin) at which the restoring torque due to the elastic constraints (be it the suspension wire or the full ensemble of chains of force in the granular) cannot be overcome. This will eventually limit all movement in a confined range of configurations.

We simplify the problem by considering separately the effect of fractional Brownian motion, on one side, and of Brownian motion evolving under the effect of an external

J. Stat. Mech. (2012) P01002

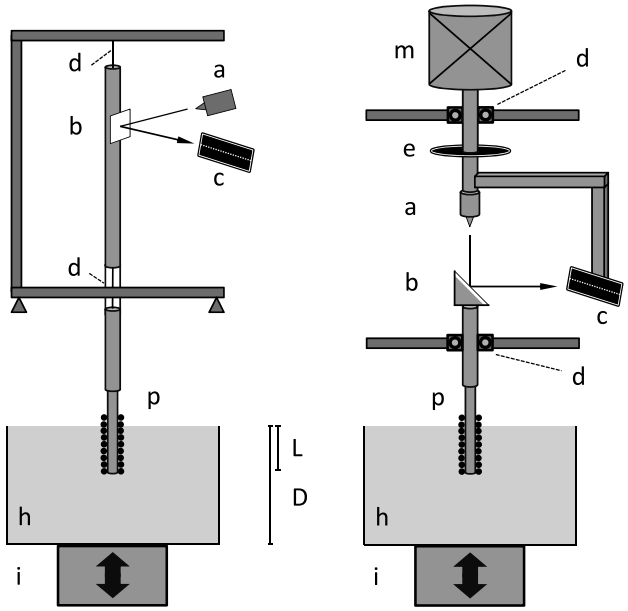

Figure 1. Sketches of the two experimental set-ups. On the left, the forced torsion oscillator configuration. On the right, the Brownian motor configuration. In both cases, a cylindrical probe is used. Glass beads, identical to those in the granular medium, are glued on the probe walls, making it sensitive to the local movements of the grains. The probe is immersed at a depth L into a granular medium of glass beads of depth D. The container, filled with the granular material, is shaken vertically by a vibration motor. An accelerometer measures the intensity of vibration, Γ. The sketch of the oscillator (left) includes: a = laser diode; b = mirror; c = position sensing photocell; d = suspension wires; p = cylindrical probe; h = granular medium; i = vibrator motor. The sketch of the Brownian motor (right) includes: a = laser diode; b = mirror; c = position-sensing photocell; d = suspension ball bearings; e = motor speed sensor; m = alignment motor; p = cylindrical probe; h = granular medium; i = vibrator motor.

potential, or constraint, on the other side. To this end, we consider a particle moving on a lattice. For a simple random walk, at each step the probability to move to the right ($\Delta = +1$) is $P(\Delta = +1) = 0.5$ and vice versa for ($\Delta = -1$). We modify the random walk simulation to take into account this phenomenon, in two very simple ways.

In the first case, we modify the probability to move in either direction, so that, at each lattice point n, the probability to move to point $n+1$ is given by $P(n \to n+1) = 0.5 - A \times n$, where A is the constraint parameter that we can choose. This contribution proportional to the distance from the origin can be interpreted as the presence of a quadratic potential. From this definition, it is clear that the simulated 'constrained' random walk does not differ from the standard one at the origin (and in the immediate neighborhoods). On the other hand, for the lattice point m such that for the chosen A we have that $Am = 0.5$, we see that it can only span the region $(-m; +m)$.

With this rule, we performed simulations for different values of the parameter A between 10^{-6} and 10^{-2}.

J. Stat. Mech. (2012) P01002

To ensure that the constraint does not introduce unwanted effects due to the 'hard-wall' constraint it imposes on the random walk, we repeated the simulation using a transition probability of sigmoidal shape: $P(n \to n+1) = 1 - (1/1 + \mathrm{e}^{-\sigma n})$. In this case, we can tune the sharpness of the sigmoid, changing the parameter σ, while ensuring that there is no hard-wall effect. We run different simulations with $10 \leq \sigma \leq 10^6$.

Simulations were run for 10^6 steps and statistical analysis was performed on 10^5 samples to get good statistics. At each fixed amount of time steps (typically 2000 or 10 000) the actual position of the random walker with respect to the origin was recorded. With these data, we constructed histograms showing the relative frequencies of finding a walker at a given distance from the origin. For each simulated configuration, we also recorded a small number of simulated time series, so that they could be studied directly with fractal analysis.

2.2. Experimental set-up

For the experimental part of this work, we consider a granular material composed of glass beads of diameter $d_\mathrm{g} = 1.1\ \mathrm{mm} \pm 10\%$. The experimental set-up is composed of two different measurement equipment: a torsion oscillator and a 'Brownian motor'. Both set-ups are sketched, respectively, in the left and right part of figure 1.

The granular medium is contained in a metallic bucket (height 96 mm, diameter 94 mm, filled to a height of approximately 65 mm), which is fastened to the moving element of a vibration motor which, in turn, is held in place by a trunnion placed on a stable support.

An accelerometer fixed on the container measures the vibration intensity. This intensity, called Γ, is defined as the square root of the acceleration band power in a frequency window between 1 Hz and 10 kHz, integrated and normalized with respect to the acceleration of gravity, g: $\Gamma = (1/g)\int A(f) f\,\mathrm{d}f$. In the simple case of a sinusoidal vibration of amplitude a_s and frequency $f_\mathrm{s} = \omega_\mathrm{s}/2\pi$, one obtains $\Gamma = a_\mathrm{s}\omega_\mathrm{s}^2/g$. In our experiments, we feed the vibration motor with a broadband signal, the spectral representation of which is a filtered white noise cut off below 70 Hz and above approximately 1 kHz. The rationale behind this choice is to reduce spurious effects (resonances, oscillations and the formation of convection cells) that appear more easily, especially at high Γ, when fixed frequency excitations are used.

We analyze the granular medium by means of a probe connected to a low-frequency torsion oscillator, or to a freely turning rod, suspended on ball bearings. The probe is a cylinder covered by a layer of glued beads, with effective radius $R_\mathrm{e} \approx 2.5$ mm, and immersed at a depth $L \approx 45$ mm.

In the case of the torsion oscillator set-up, the probe is left free to move, with constraints arising from the interaction with the granular material and the suspension wires. The global effect of these interactions on the probe can be summarized as follows:

(a) *A local restoring coefficient.* This arises partly from the actual spring constant of the suspension (in the torsion oscillator set-up) and partly from the interactions between the granular medium and the probe. In the high Γ, fluid condition, the apparent elastic modulus ascribed to the granular interaction is approximately three

to four times higher than the one coming from the suspension. As the vibration strength is reduced, the granular becomes much stiffer and the ratio between the two contributions can rise up to 100:1 and above.

(b) *A damping effect due to viscous friction.* This comes from both mechanical loss in the suspension and from the dissipation of energy within the granular sample. Since the damping due to the suspension is always lower by at least a factor of 100 with respect to the damping due to grain interaction, we will only consider the latter.

(c) A white noise term (in the Langevin sense), responsible for the Brownian behavior of the probe.

Typical angular displacements during the experiments do not exceed 0.01 radians. This corresponds approximately to a maximum linear displacement of 0.1 mm of any point at the surface of the probe.

Moisture-induced aging effects [12, 13], and interstitial gas effects [14], are not observed due to the relatively large bead size used here, and measurements are performed under an uncontrolled atmosphere. In order to control compaction effects [15], all measurements are taken in the same conditions, e.g. starting from a granular material shaken at $\Gamma \approx 6$ with a large band signal (f_s between 70 and 1000 Hz) for 10–20 min. In these conditions, compaction effects have characteristic times of the order of 1 h, and are apparently negligible in the timescale of the experiments. These last approximately 2 or 3 min. In some cases, the dielectric nature of the beads could cause perturbations (electric repulsion due to friction-induced polarization), but our full-metal assembly keeps this effect under control.

The angular position of the oscillator, $\theta(t)$, is optically detected with a linear analog photocell. The optical arm (the distance between the rotation axis and the photocell) is, in this case, approximately 70 cm. Resulting position data are recorded at sampling rates of 10 or 20 kHz with a National Instrument NIDaQ 6009 digital voltmeter and are stored on a computer. The electrical noise level do not exceed the value of 1% in the most delicate measurement conditions.

We performed the experiments with vibration levels in the range $0.01 < \Gamma < 5$. For each Γ, we recorded a 600 or 1200 s long time series.

Finally, in order to assess the possible influence of the torsional constraint due to the pendulum suspension, we repeated the experiment with a slightly different configuration, often referred to as a 'Brownian motor' set-up. In this case, the probe is kept in place by two ball bearings and is therefore free to move (again, with only one degree of freedom) under the effect of the interaction with the granular medium.

The movement of the probe is again measured with the photocell. The optical arm, in this case, is approximately 8 cm. The resulting signal is electronically decomposed into average drift (slow movement) and fluctuations (fast movement). Via a feedback circuit, the average drift is fed to the electric motor placed on top of the structure. The average drift of the probe is therefore compensated by turning the upper section, so that, on average, the reflected laser beam always falls on the center of the photocell. The fluctuations are sampled at high frequency in the same way it was done in the torsion oscillator set-up.

J. Stat. Mech. (2012) P01002

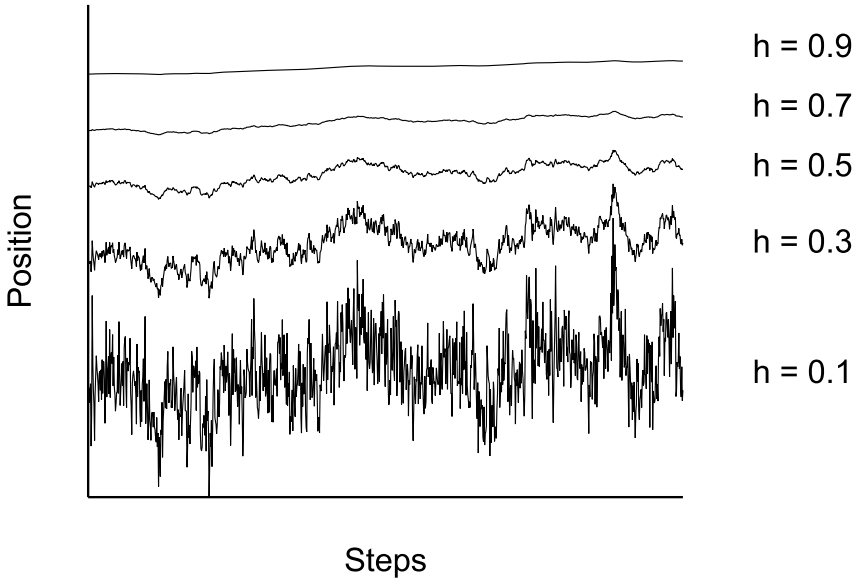

Figure 2. Representation of different simulated FBM obtained with five values of the Hurst exponent. In this case, the fractal dimension d is related to the Hurst exponent h by the equation $d = 2 - h$ (as discussed in the main text). A small Hurst exponent has a higher fractal dimension and a rougher surface, while a larger Hurst exponent has a smaller fractional dimension and a smoother surface. The data were obtained by simulating fractional Brownian motions with different h exponents, but keeping the random seed fixed [23]. These simulated curves show strong similarities to the experimental time series of figure 4.

2.3. Fractal analysis of time series

Our experimental time series were studied by the means of fractal analysis. This approach was originally proposed by Mandelbrot [16] and consist in calculating the so-called fractal dimension of a given signal.

One of the inherent advantages of this method is that it can be used to extract stable observables from data that cannot be easily treated otherwise (for example, with Fourier analysis). More specifically, our experimental data are time series of the angular position of the probe. These represent, therefore, one-dimensional trails as a function of time.

In the simplest case of one-dimensional Brownian motion, it has been shown that, with probability 1, the graph of a Brownian sample function has a dimension D equal to 1.5. A theorem [17] demonstrates that this fact is directly related to the theory of diffusion. In Brownian motion the dynamics of diffusion obey the equation $\langle x \rangle \propto t^h$, with $h = 0.5$, so that $D + h = 2$.

However, the mathematical conditions that define a Brownian motion can be relaxed and the transition probability can be modified to introduce a term that locally either opposes the movement of the Brownian object, or that propels it. Such modifications directly translate into a visible feature of the resulting graph. A propulsive effect (for example, due to inertial phenomena) tends to smoothen out the graph, while constraining effects make the trails look 'noisier'. This effect is exemplified in figure 2.

J. Stat. Mech. (2012) P01002

This phenomenon is related to the fractal dimension of the Brownian motion by another theorem [17] stating that, with probability 1, the graph of an index h Brownian sample function $X_h : [0, 1] \to \mathbb{R}$ has a dimension $2 - h$.

This theorem allows us to interpret our experimental and simulated data in regard to the concept of anomalous diffusion [18, 19, 1]. In short, one system is said to show (normal) diffusion when the variance of some position observable scales linearly as a function of time (for large enough times). When this is no longer true, we speak of anomalous diffusion. In this case the square root of the variance of the observable position no longer increases as $\sigma_x \propto \sqrt{t}$, but instead behaves as a power law with exponent $h \neq 1/2$. In this context, the Brownian motion is said to be 'fractional' (abbreviated to FBM) and the exponent h is often called the 'Hurst exponent'. This fact, and general properties of anomalous diffusion, have been widely studied in other works, such as the review by Bouchaud and Georges [19], and also to the studies of Balakrishnan [18], Schneider [20], Saichev [21] and Barkai [22].

3. Results

This section is composed of two parts. In the first one, we discuss the simulated data. This part will be useful to elucidate a few key features of our system, and to introduce concepts useful to further discuss our experimental measurements. The experimental work is presented in the second part.

3.1. Simulation

As discussed before, our simple model consists of a random walk with a transition probability, which is modified as a function of the position. When the simulations are run, we generate a large number of instances of random walks with identical parameters (constraint, number of steps, etc). For a given set of parameters we use the large number of instances to construct the position frequency histograms. We repeat this for a large number of intermediate time steps between the start and end. Furthermore, for every set of parameters, a few simulated instances (or 'realizations') are recorded, for further analysis. We can now make a few remarks.

First, we observe that the frequency histograms constructed from the simulated time series are Gaussians, even for the strongest constraints. We used this fact to impose a stronger constraint on data analysis: the variance parameter is computed, at each step, by fitting a Gaussian curve to the histogram. The same procedure will then be applied to the experimental time series, where a Gaussian distribution is not expected *a priori*. This will be discussed in section 3.2, but we can anticipate that the experimental data also behave in a similar way.

Second, the addition of this constraint breaks the usual diffusion rule $\langle \Delta \rangle = \sqrt{t}$ for large times, as the random walker starts exploring the regions far from the origin where the constraint becomes larger. The limit width of the distributions can be computed and (as expected) it is proportional to the square root of the constraining parameter. We also noticed that the choice of the constraining method (linear spring or sigmoidal correction) does not influence the results. A comparison between nonconstrained and constrained data is shown in figure 3. This graph allows for an interesting comparison

J. Stat. Mech. (2012) P01002

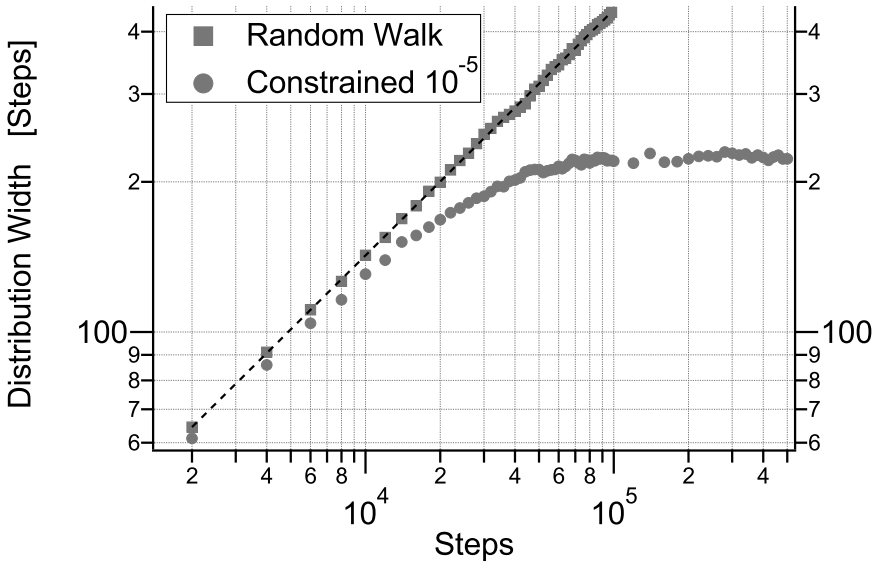

Figure 3. Evolution of the width of the simulated distributions for the standard random walk and for a constraint parameter $A = 10^{-5}$. The unconstrained random walk (crosses) shows the classic diffusion rate $\propto\sqrt{x}$, indicated by the dashed black line. The constrained data (circles) instead saturates to a fixed width. This was computed up to step 10^6. The corresponding experimental time series, shown in figure 6, indicate a similar behavior.

with its experimental counterpart shown in figure 6, which will be discussed in section 3.2. We can therefore conclude observing that the presence of a constraining force applied on a Brownian particle lowers the diffusion exponent h.

3.2. Experiment

It is not trivial to directly repeat the analysis performed on simulated data when we consider experimental time series. This is for two main practical reasons. First, it will take too long (centuries) to record the same number of time series needed to perform the time averages as we just did for the simulation. Second, it is true that we can perform the ensemble averages: in this case it means computing the histogram of the 'number of visits at location x' as a function of time. However, the system has a non-ergodic behavior at the timescales which are experimentally accessible. In fact, as the granular approaches complete jamming ($\Gamma \to 0$), the probe spends exponentially growing times in each consecutive position (following granular rearrangement). Since the characteristic times diverge, there is simply no way to access the quantity of data necessary to get good statistics, in order to apply conventional analytical approaches. This is evident in the experimental data shown in figure 4. Here we show three typical time series, obtained with the cylindrical probe, for different values of the vibration level Γ. The recorded trails of the probe change as a function of Γ. The overall behavior reminds us closely of the fractional Brownian trails of figure 2: in the low Γ region, the probe is strongly confined and it oscillates frequently around the same equilibrium positions; as the vibration intensity increases, the constraining effect of the granular medium becomes less important and the evolution becomes smoother. We anticipate that this property can

J. Stat. Mech. (2012) P01002

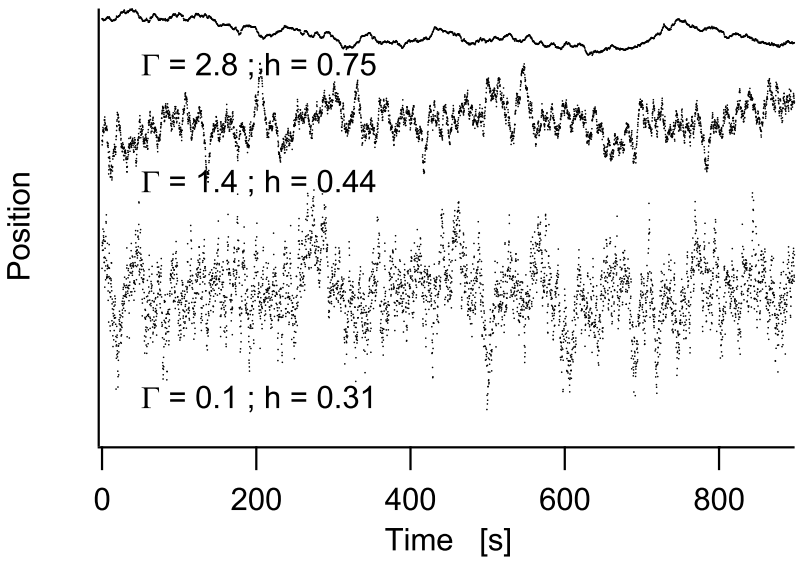

Figure 4. Three experimental time series obtained with different levels of vibration Γ (as indicated). Side-by-side comparison can be made with the simulated fractional Brownian trails shown in figure 2, suggesting that our system behaves as a constrained random walk (the relative amplitudes have been scaled). For each curve we also report the corresponding Hurst exponent as defined in section 4.

be described with the Hurst exponent (also shown besides each curve). This observable will be discussed in detail in section 4.

The experimental data is further analyzed as follows. For each level of vibration intensity Γ, we record a time series. At any given time T, after the beginning of the measurement, a given angular region will then have been swept. We divide this region into small slices and we compute the occupancy histogram considering the amount of time spent in a given slice, from $t = 0$ to T. Therefore, for each time T, we can construct an histogram. We split the time series in 1 s interval. The histograms are then fitted with a Gaussian curve. We note that the computation of the variance of the data is performed via the Gaussian fit to keep consistency with the simulated time series (where the Gaussian shape of the distribution is guaranteed by the CLT). As an example, we show the fitted Gaussian width for $\Gamma = 0.55$ in figure 5.

Finally, figure 6 shows the final width of the time-series occupancy histograms as a function of the vibration intensity Γ. In the strong vibration regime, the swept area appears to be constant. It starts to decrease as the intensity of shaking is reduced, but in this case the noise level becomes much more important.

4. Discussion

4.1. Defining the fractal dimension: Hurst exponent

Once the time series are measured, the fractal dimension and the Hurst exponent can be inferred. The fractal analysis performed in this work was done with the software toolbox

J. Stat. Mech. (2012) P01002

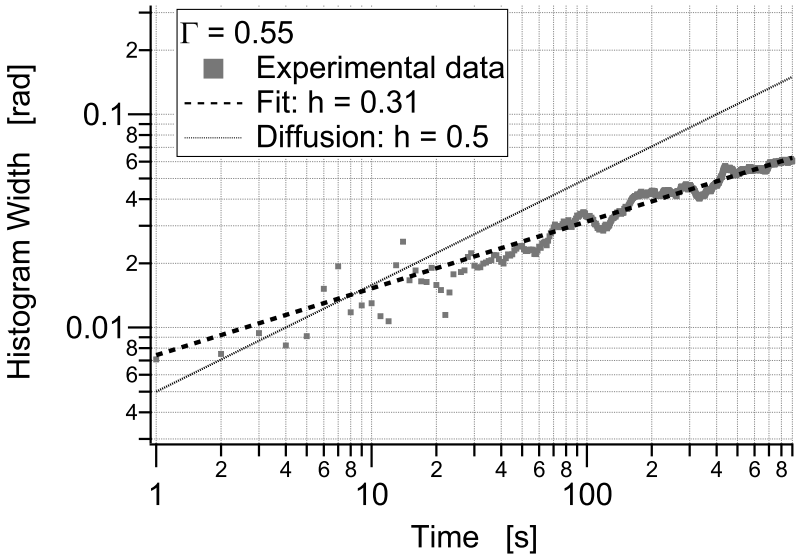

Figure 5. Example of the broadening of the region spanned in the experimental time series. The data, though noisy, indicate that the probe sweeps an increasing area, with an anomalous diffusion exponent.

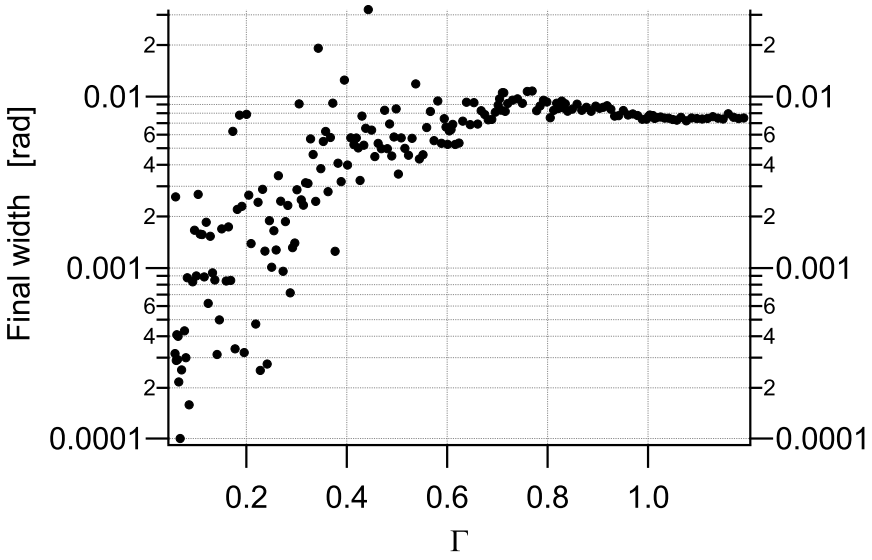

Figure 6. Final width of the histograms of the experimental time series. The data correspond to the final width of all histograms computed as in the example of figure 5. For the lower vibrations, the swept area increases with the vibration intensity. However, as the vibrations increase, the width of the histograms stabilizes. In this region, the computation of the box dimension is more sensitive to the changes in the dynamics, as can be seen in figure 8.

J. Stat. Mech. (2012) P01002

FracLab for the Matlab platform. It is available as open source software and is developed by the Regularity team of INRIA—CNR Saclay (see [24, 25]).

With the help of this package, it is possible to compute two different approximations of the Hausdorff dimension of a time series. The simplest, and less computationally intensive is the well-known box counting (or simply 'box') method [26]. Unfortunately, this method has the disadvantage of converging very slowly to the fractal dimension, as the length of the considered time series is increased. This means that, if the considered time series are not long enough, they only could give a rough estimate of the correct box dimension. We performed some simulations and we observed worst-case deviations by up to 15%, by comparison with expected theoretical values. This fact has been already discussed in the past [27].

In principle one could use other, more powerful, methods, such as the 'regularization' method provided in the same software package. Unfortunately, the regularization technique is quite computationally intensive and, in the current implementation, is not suitable to systematic analysis of experimental data.

4.2. Simulations

We first performed some analysis on the data coming from our simulations. The computed Hurst exponents are shown in figure 7. In this case, we show the data obtained with a linear constraint. We considered one instance of a simulated random walks for different values of the constraint parameter A. To allow an easier comparison with experimental data, where the effective constraint due to the granular material decreases with increasing vibrations, we plotted the Hurst exponent as a function of the inverse of the constraint parameter A. The ordinate shows the estimates for the Hurst exponent h obtained with the box method on 10^4 and 10^6 steps long random walks (respectively indicated by the gray and black markers).

For the case $A \to 0$ (pure Brownian motion) we know that the Hurst exponent must be exactly $h = 0.5$. If we consider the 10^6 steps dataset (black), the agreement with the theory is good, although not perfect: the data indicate that the exponent is slightly overestimated. For $A = 0$ we obtain $h = 0.56 \pm 2.0\%$; this is indicated on the graph by the dashed horizontal line in the right-hand part. The estimations of h grow worse as we shorten the considered length to 10^4 steps (gray dataset).

As discussed above, further increase in the number of steps has a progressively smaller effect on the computation of h. From these observation, we conclude therefore that a dataset composed of 10^6 already allow a reasonable estimate of the Hurst exponent.

If we now focus on this dataset, we can observe the evolution of h as a function of A. As already noted, the limit $A = 0$ corresponds to a normal Brownian motion. When the constraint increases, on the other hand, we observe that the Hurst exponent decreases as A increases. In the region defined by $10^{-5} \leq A \leq 10^{-3}$, the data suggests an approximate decrease of 0.15 per decade. This is highlighted by the dotted–dashed diagonal line, which is a guide for the eye. Finally, below this region, for $A > 10^{-2}$, the effects of the constraint become very large, so that the region of space available for the random walk is extremely reduced. In this limit, the Hurst exponent progressively loses importance, since the system becomes only sensitive to the random term.

J. Stat. Mech. (2012) P01002

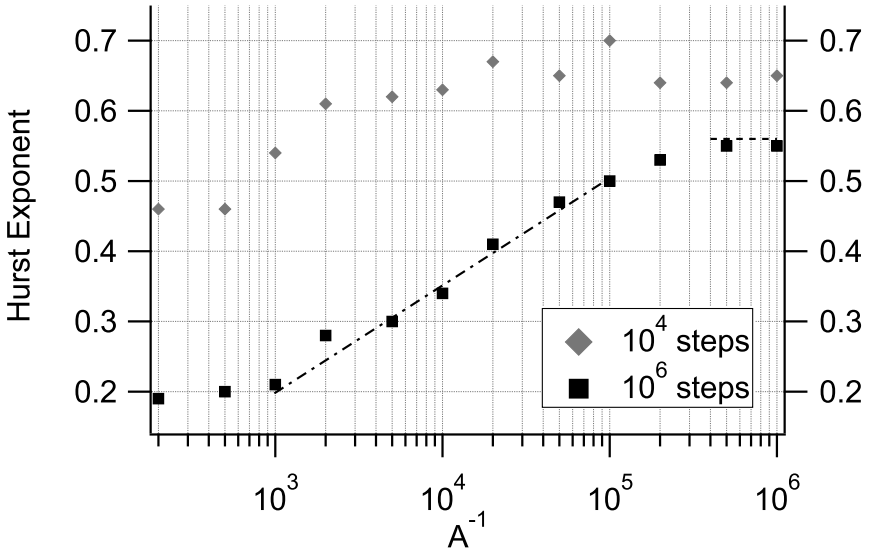

Figure 7. Computed values for the Hurst exponent h, plotted as a function of the inverse of the constraint parameter A. We considered one instance of a simulated random walk for each value of A. The exponent h is estimated with the box method over a RW of 10^4 (gray markers) and 10^6 steps (black markers). Short time series lead to overestimation of h; this improves, albeit very slowly, with the size of the datasets. The horizontal dashed line indicates h obtained in the limit case $A = 0$ for a 10^6 step time series. The data suggest that in the region $10^{-5} \leq A \leq 10^{-3}$ h decreases by approximately 0.15 as A increases of a factor 10. This interesting fact is highlighted by the diagonal dotted–dashed line.

It is also important to note that our simulation technique does not allow us to generate propelled Brownian trails with an exponent h larger than 0.5. This happens because our simple model constructs the 1D random walks step by step, and the constraint is directly introduced as a bias in the transition probability $P(x)$. However, unfortunately, for technical reasons there is no simple way to simulate an FMB in which the stepwise transition probability can be modified by a given amount (as we did with the simple random walker). For this reason our simulated data can only span the region $0 < h \leq 0.5$.

Despite these limitations, we can conclude this section with the following three key observations. First, the simulations have allowed us to assess the reliability of the estimation of the Hurst exponent via the box dimension. The simulation data indicate that the computed values do not substantially depart from the expected theoretical value, provided that the time series are long enough that the computation algorithms can converge to a reasonable estimation. Second, the generation of simulated time series allows us to compute the variance of the position distribution in a well-defined framework and allows a direct comparison with experimental data. This can be seen by observing figures 3 and 6. Third, the simulated data clearly show that the addition of a constraining effect makes the time series look more 'irregular', thereby increasing their dimensionality; this fact can be meaningfully described with the Hurst exponent.

J. Stat. Mech. (2012) P01002

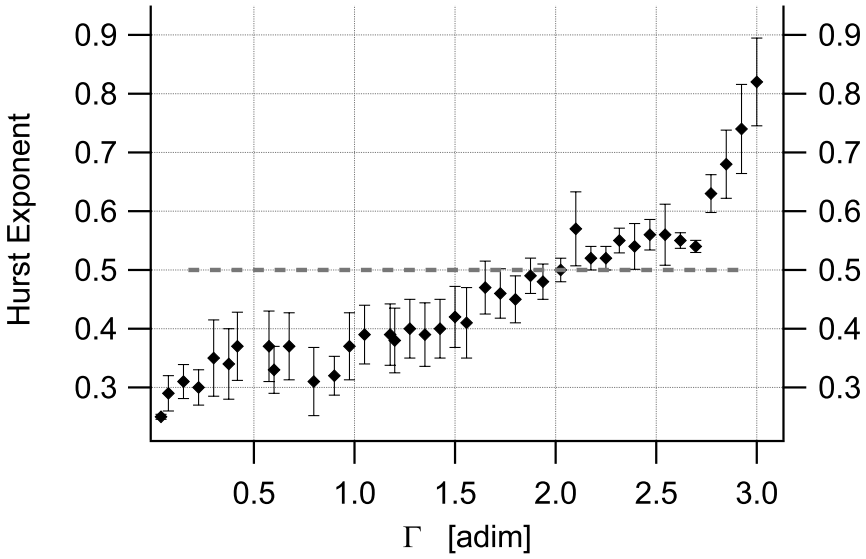

Figure 8. Hurst exponent for experimental time series obtained with the torsion oscillator set-up. The data are plotted as a function of the average acceleration intensity Γ and were computed with the box dimension method. The graph shows that for strongly vibrated system the exponent is compatible with a superdiffusive behavior. As the strength of the excitations is reduced, the system 'slows down' to a jamming regime where diffusion is inhibited.

4.3. Experimental data

In figure 8 the computed Hurst exponent is plotted as a function of Γ. It is clear that, as the vibration intensity is decreased, the average rate of diffusion is reduced. As discussed in section 4.2, the use of the box method can introduce inaccuracies in the results. However, a slight systematic deviation does not significantly change the interpretation of the data.

At higher vibration intensities, the granular medium is fluidized. In this phase, dynamic effects due to convection influence the motion of the probe and superimpose on a simple random walk. In this region, we have a 'superdiffusive' behavior: the Hurst exponent is greater than 0.5.

As the vibration intensity is lowered, we approach the jamming transition. As motion slows down, the Hurst exponent lowers, as convection effects become less and less important. This can clearly be seen as the apparent roughness of the time series becomes more pronounced (figure 4).

Finally, as the vibration is further reduced, we reach the jamming phase and the Hurst exponent becomes lower than 0.5. This fact suggests the following interpretation. In the jamming region, the probe is subject to the movement of a large number of granular particles. However, with decreasing vibrations, the network of chains of forces in the granular medium becomes more and more complex. In this situation, the overall position of the probe can change only if a large scale rearrangement event takes place. If such a rearrangement does not happen, the probe has a greater probability of going back to the previous position. Therefore, we obtain a behavior similar to a constrained random walk.

J. Stat. Mech. (2012) P01002

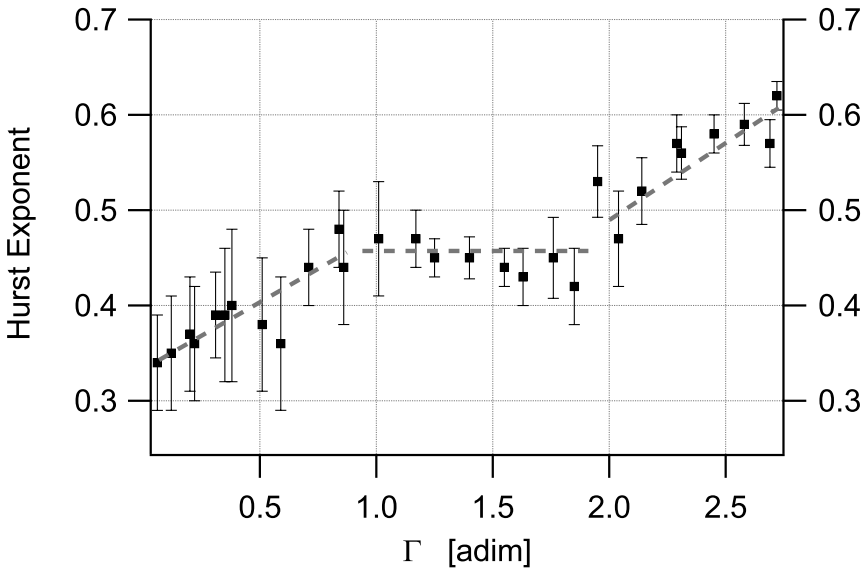

Figure 9. Hurst exponent for experimental time series, obtained with the torsionally unconstrained apparatus ('Brownian motor'). Apart from this, the data were obtained otherwise using the same method as those shown in figure 8. In this case, despite the larger dispersion of the data, a plateau can be seen for $h \approx 0.5$ in the region $1 < \Gamma < 2$.

In other words, the dynamics of the system is dominated by Lévy flights and/or extreme event statistics [28, 29].

One interesting observation is the fact that, as the Hurst exponent decreases, apparently no plateau is reached. We attribute this fact to the presence of the weak restoring coefficient due to the torsion suspension, which is always constraining the movement of the probe independently of the condition of the granular system.

As discussed in the experimental set-up, the torsion constraint due to the suspension wires is much smaller than the effect of jammed granular media, but it accounts for around 1/3 of the 'apparent' restoring force of a fluidized medium. In order to fully assess the effect of this external constraint, we consider the data obtained with the free rotating, 'Brownian motion', set-up. In this case, the probe is suspended by two ball bearings that allow rotational motion with very little friction. In this configuration, a symmetric probe can rearrange freely in any direction, not being subject to a preferential spatial direction (due to the torsion spring). We note that all the other experimental conditions (granular medium, probe, spectrum of the vibration noise, etc) are otherwise identical to those employed in the torsion oscillator measurements.

The resulting data are shown in figure 9. First, we have to note that, for sensitivity reasons, there is a larger scatter of the data points. In fact, the optical arm of the Brownian motor set-up is, currently, approximately nine times shorter than that of the torsion pendulum. For this reason, the signal-to-noise ratio of the Brownian motor installation is smaller. Considering similar displacements in the granular medium, and a similar amount of electronic noise in both photocell electronic chains, this fact explains the larger scatter of figure 9 with respect to figure 8.

J. Stat. Mech. (2012) P01002

However, in this case we can clearly see that the graph shows three distinct regions. For strong vibrations, $\Gamma > 2$, h is larger than 0.5 and increases as the system becomes more and more prone to convection effects. The corresponding rightmost, dashed, gray line corresponds to a least-squares fit (in this case, the slope is approximately $m = 0.16$). If the vibration intensity is reduced, for vibrations of intermediate strength $1 < \Gamma < 2$, the Hurst exponent stabilizes and reaches a plateau (indicated by the central gray dashed line, $h \approx 0.46$). In this region, it appears that the system evolves as a normally diffusing Brownian particle, if the deviation from the expected value of 1/2 can be attributed to numerical approximations. This region is not present in figure 8, as the constraining effect of the torsion suspension is relatively important. Finally, as Γ becomes smaller than 1, the system starts to jam and the Hurst exponent decreases (the leftmost gray dashed line is again obtained by a least-squares fit of a straight line of slope $m = 0.13$). We note that a similar phenomenon, showing a crossover between simple diffusion and a caging behavior, has been observed in an analogous (albeit two-dimensional) system [30].

We can now compare the Hurst exponent obtained with the simulations with the one obtained with the experiments (figure 9). Our simulations only allow us to study the dynamical region where $h < 0.5$. In the experimental data, this corresponds approximately to the vibration intensities window $0 \leq \Gamma \leq 1$, where we observe an increase of h as Γ increases. If we focus in this region, the simulations (see figure 7) indicate that, for values of constraint in the range $10^{-5} \leq A \leq 10^{-3}$, the Hurst exponent h decreases by approximately 0.15 for each tenfold increase (decade) of the constraint parameter A. The experimental analog in figure 9 gives $h_{\Gamma=0} \approx 0.35$ and $h_{\Gamma=1} \approx 0.55$: therefore, we observe a variation $\Delta h = 0.2$. If this change of the experimental Hurst exponent can be attributed to an increase of a constraining force acting on the probe (and ultimately depending on the granular medium), this would correspond to a change of $10^{0.2/0.15} \approx 20$ times in the constraint value. While this approach only provides rough estimates is nonetheless very interesting. With a different technique, the evolution of the stiffening of a granular system as a function of Γ has been observed [9]. We can see that, under the same experimental conditions, the measured change in stiffness has the same magnitude.

As a final remark, we remind that the effect of electronic noise is negligible, since in typical measurements it accounts for less than 1% of the mechanical signal. We also estimated that the Hurst exponent of the signal of this electronic noise is 0.50. As expected, the electrical noise in our cell has a random-walk-like behavior.

Further development of this work will involve a more detailed characterization of the freely rotating system. One field of interest will be the study of the dynamics of asymmetric probes. Asymmetric geometries can be put into rotation by rectification of granular collision noise [31]. In this latter case the interaction is between 'macroscopic' constant speed movement and 'microscopic' Brownian fluctuations.

5. Conclusion

We have applied fractal analysis techniques to the time series of a torsion pendulum immersed in vibrated granular materials.

We have, for the first time, given direct evidence that the dynamics of such a system is well described by the Brownian motion model.

J. Stat. Mech. (2012) P01002

Further analysis and comparison with a very simple constrained random walk allows us to interpret the dynamics of the probe as a fractional Brownian motion, with a well-defined Hurst exponent.

Therefore, we can prove that a torsion probe immersed in a vibrated granular system behaves as an anomalously diffusing Brownian-like particle. Its dynamics is described by a Hurst exponent that depends on the intensity of the vibrations imposed on the granular medium and, if present, on an externally imposed constraint. In general, we observe that at high vibration intensities the system is superdiffusive and is eventually dominated by convection, while at low vibration intensities it describes a constrained random walk. If there is no significant externally applied torque, as is the case for the Brownian motor set-up, an intermediate region appears where the probe exhibits regular (nonanomalous) diffusion.

This normally diffusing region is not present in the data obtained with the torsion pendulum, where the Hurst exponent is always smaller than 0.5 in the $1 < \Gamma < 2$ range. This means that the system becomes sensitive to the constraining effect of the suspension wires.

Furthermore, in both cases, these data systematically show an Hurst exponent smaller than 0.5, when Γ is sufficiently small, which is related to a constrained random walk. It is interesting to notice that, in these conditions, there are no inertial effects (which would be signaled by an Hurst exponent greater than 0.5).

Acknowledgments

AS would like to thank Riccardo Balzan for discussions and advice; Iva Tkalčec for the discussions, advices and technical help; Antonio Gentile and Nicolas Turin for technical help. This work was financed by SNF (Swiss National Science Fund) grant no. 200020_126534. The authors declare that they have no competing interests.

References

[1] de Gennes P G, *Granular matter: a tentative view*, 1999 *Rev. Mod. Phys.* **71** S374
[2] Jaeger H M, Nagel S R and Behringer R P, *Granular solids, liquids, and gases*, 1996 *Rev. Mod. Phys.* **68** 1259
[3] Corwin E I, Jaeger H M and Nagel S R, *Structural signature of jamming in granular media*, 2005 *Nature* **435** 1075
[4] Debenedetti P G and Stillinger F H, *Supercooled liquids and the glass transition*, 2001 *Nature* **410** 259
[5] Dauchot O, *Glassy behaviours in athermal systems, the case of granular media: a tentative review*, 2007 *Ageing and the Glass Transition* (*Springer Lecture Notes in Physics vol 716*) ed M Henkel, M Pleimling and R Sanctuary (Berlin: Springer) pp 161–206
[6] Duran J, 2000 *Sands, Powders, and Grains: an Introduction to the Physics of Granular Materials* (New York: Springer) Partially Ordered Systems
[7] Mayor P, D'Anna G, Barrat A and Loreto V, *Observing brownian motion and measuring temperatures in vibration-fluidized granular matter*, 2005 *New J. Phys.* **7** 28
[8] D'Anna G, Mayor P, Barrat A, Loreto V and Nori F, *Observing brownian motion in vibration-fluidized granular matter*, 2003 *Nature* **424** 909
[9] Sellerio A L, Mari D, Gremaud G and D'Anna G, *Glass transition associated with the jamming of vibrated granular matter*, 2011 *Phys. Rev.* E **83** 021301
[10] D'Anna G and Gremaud G, *Vogel–Fulcher–Tammann-type diffusive slowdown in weakly perturbed granular media*, 2001 *Phys. Rev. Lett.* **87** 254302
[11] Radjai F and Roux S, *Turbulentlike fluctuations in quasistatic flow of granular media*, 2002 *Phys. Rev. Lett.* **89** 064302

J. Stat. Mech. (2012) P01002

[12] Bocquet L, Charlaix E, Ciliberto S and Crassous J, *Moisture-induced ageing in granular media and the kinetics of capillary condensation*, 1998 *Nature* **396** 735
[13] D'Anna G, *Mechanical properties of granular media, including snow, investigated by a low-frequency forced torsion pendulum*, 2000 *Phys. Rev.* E **62** 982
[14] Pak H K, Van Doorn E and Behringer R P, *Effects of ambient gases on granular materials under vertical vibration*, 1995 *Phys. Rev. Lett.* **74** 4643
[15] Knight J B, Fandrich C G, Lau C N, Jaeger H M and Nagel S R, *Density relaxation in a vibrated granular material*, 1995 *Phys. Rev.* E **51** 3957
[16] Mandelbrot B B, 1983 *The Fractal Geometry of Nature* (New York: Freedman)
[17] Falconer K, 1990 *Fractal Geometry: Mathematical Foundations and Applications* (New York: Wiley)
[18] Balakrishnan V, *Anomalous diffusion in one dimension*, 1985 *Physica* A **132** 569
[19] Bouchaud J-P and Georges A, *Anomalous diffusion in disordered media: statistical mechanisms, models and physical applications*, 1990 *Phys. Rep.* **195** 127
[20] Schneider W R and Wyss W, *Fractional diffusion and wave equations*, 1989 *J. Math. Phys.* **30** 134
[21] Saichev A I and Zaslavsky G M, *Fractional kinetic equations: solutions and applications*, 1997 *Chaos* **7** 753
[22] Barkai E and Fleurov V N, *Generalized Einstein relation: a stochastic modeling approach*, 1998 *Phys. Rev.* E **58** 1296
[23] Peitgen H-O and Saupe D, 1988 *The Science of Fractal Images* (New York: Springer)
[24] Roueff F and Levy Vehel J, *A regularization approach to fractional dimension estimation*, 1998 *Proc. Fractals'98 (Malta)*
[25] Lévi Véhel J and Legrand P, 2004 *Thinking In Patterns. Fractals and Related Phenomena in Nature* (Vancouver: World Scientific) pp 321–3
[26] Simanca S R and Sutherland S, 2002 *Mathematical Problem Solving With Computers* (New York: University at Stony Brook)
[27] Feng Z, Zuo M J and Chu F, *Application of regularization dimension to gear damage assessment*, 2010 *Mech. Syst. Signal Process.* **24** 1081
[28] Lévy P, *Wiener's random function, and other Laplacian random functions*, 1951 *Proc. 2nd Berkeley Symp. on Mathematical Statistics and Probability, 1950* (Berkeley and Los Angeles: University of California Press) pp 171–87
[29] Lévy P, 1992 *Processus Stochastiques et Mouvement Brownien* ed J Gabay, and Sceaux, Followed by a note by M Loève, Reprint of the second (1965) edition (Paris: Gauthier-Villars)
[30] Reis P M, Ingale R A and Shattuck M D, *Caging dynamics in a granular fluid*, 2007 *Phys. Rev. Lett.* **98** 188301
[31] Balzan R, Dalton F, Loreto V, Petri A and Pontuale G, *Brownian motor in a granular medium*, 2011 *Phys. Rev.* E **83** 031310

J. Stat. Mech. (2012) P01002